

Deep Generative Modeling of LiDAR Data

Lucas Caccia^{1,2}, Herke van Hoof^{1,4}, Aaron Courville^{2,3}, Joelle Pineau^{1,2,3}

Abstract—Building models capable of generating structured output is a key challenge for AI and robotics. While generative models have been explored on many types of data, little work has been done on synthesizing lidar scans, which play a key role in robot mapping and localization. In this work, we show that one can adapt deep generative models for this task by unravelling lidar scans into a multi-channel 2D signal. Our approach can generate high quality samples, while simultaneously learning a meaningful latent representation of the data. Furthermore, we demonstrate that our method is robust to noisy input – the learned model can recover the underlying lidar scan from seemingly uninformative data.

I. INTRODUCTION

One of the main challenges in mobile robotics is the development of systems capable of fully understanding their environment. This non-trivial task becomes even more complex when sensor data is noisy or missing. An intelligent system that understands the data generation process is much better equipped to tackle inconsistency in its sensor data. There is significant potential gain in having autonomous robots equipped with data generation capabilities which can be leveraged for reconstruction, compression, or prediction of the data stream.

In autonomous driving, information from the environment is captured from sensors mounted on the vehicle, such as cameras, radars, and lidars. While a significant amount of research has been done on generating RGB images, relatively little work has focused on generating lidar data. These scans, represented as an array of three dimensional coordinates, give an explicit topography of the vehicle’s surroundings, potentially leading to better obstacle avoidance, path planning, and inter-vehicle spatial awareness.

To this end, we leverage recent advances in deep generative modeling, namely variational autoencoders (VAE) [1] and generative adversarial networks (GAN) [2], to produce a generative model of lidar data. While the VAE and GAN approaches have different objectives, they can be used with Convolutional Neural Networks (CNN) [3] to extract local information from nearby sensor points.

Unlike other approaches for lidar processing, we do not convert the data to images or voxel grids [4] [5]. Instead, we work directly with point cloud coordinates. This data format is more memory efficient, and is therefore less expensive to process and generate. This property aids real-time input processing, which can be helpful for self-driving vehicles.

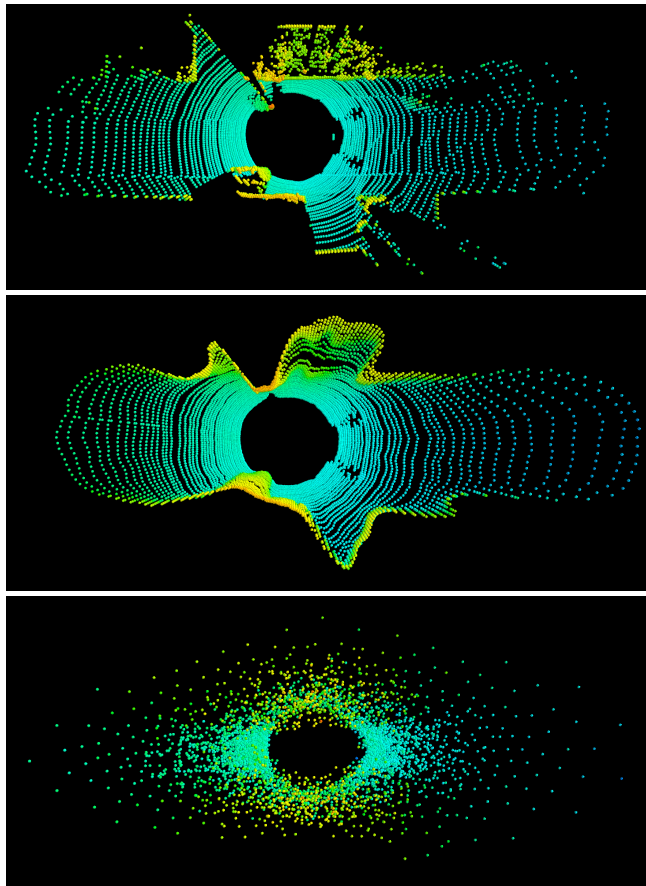


Fig. 1: Best viewed in color. Top: real LiDAR sample from the test set. Middle: reconstruction from our proposed VAE. Bottom: reconstruction from the baseline model.

The main contribution of this paper is to provide a method for *raw* lidar data generation that requires minimal human craftsmanship. In other words, our work enables lidar point cloud generation in a fully unsupervised fashion. To the best of our knowledge, no previous attempts have been made to tackle this problem. Experimental results using the standard KITTI dataset show that the method can synthesize lidar data that preserves essential structural properties of the scene.

II. RELATED WORKS

A. Lidar processing using Deep Learning

The majority of papers applying deep learning methods to lidar data present discriminative models to extract relevant information from the vehicle’s environment. Dewan et al. [4] propose a CNN for pointwise semantic segmentation to distinguish between static and moving obstacles. Caltagirone

¹ Reasoning and Learning Lab, School of Computer Science, McGill University

² MILA, Montreal Institute for Learning Algorithms

³ CIFAR Fellow

⁴ University of Amsterdam

et al. [6] use a similar approach to perform pixel-wise classification for road detection. Both papers use image representations of the lidar input, which holds less information than raw lidar scans. To leverage the full 3D structure of the input, Bo Li [7] uses 3D convolutions on a voxel grid for vehicle detection. However processing voxels is computationally heavy, and does not leverage the sparsity of LiDAR scans.

To address this issue, several papers [8]–[11] use a bijective mapping from 3D point cloud into a 2D point map, similar to polar coordinates, where (x, y, z) coordinate are encoded as azimuth and elevation angles measured from the origin. Using such a bijection lies at the core of our proposed approach for generative modeling of lidar data.

B. Grid-based lidar generation

An alternative approach for generative modeling of lidar data is from Ondruska et al [12]. They train a Recurrent Neural Network for semantic segmentation and convert their input to an occupancy grid. More relevant to our task, they train their network to also predict future occupancy grids, thereby creating a generative model for lidar data. Their approach differs from ours, as we operate directly on raw coordinates. This not only reduces preprocessing time, but also allows us to efficiently represent data with non-uniform spatial density. We can therefore run our model at a much higher resolution, while remaining computationally efficient.

C. Point Cloud Generation

A recent line of work [13]–[16] considers the problem of generating point clouds as *unordered sets* of (x, y, z) coordinates. This approach does not define an ordering on the points, and must therefore be invariant to permutations. To achieve this, they use a variant of PointNet [17] to encode a variable-length point cloud into a fixed-length representation. This latent vector is then decoded back to a point cloud, and the whole network is trained using permutation invariant losses such as the *Earth-Mover’s Distance* or the *Chamfer Distance* [16]. While these approaches work well for arbitrary point clouds, we show that they give suboptimal performance on lidar, as they do not leverage the known structure of the data.

III. TECHNICAL BACKGROUND : GENERATIVE MODELING

The underlying task of generative models is density estimation. Formally, we are given a set of d -dimensional i.i.d samples $X = \{x_i \in \mathbb{R}^d\}_{i=1}^m$ from some unknown probability density function p_{real} . Our objective is to learn a density p_θ where $\theta \in \mathcal{F}$ represents the parameters of our estimator and \mathcal{F} a parametric family of models. Training is done by minimizing some distance \mathcal{D} between p_{real} and p_θ . The choice of both \mathcal{D} and the training algorithm are the defining components of the density estimation procedure. Common choices for \mathcal{D} are either f -divergences such as the Kullback-Liebler (KL) divergence, or Integral Probability Metrics (IPMs), such as the Wasserstein metric [18]. These

similarity metrics between distributions usually come with specific training algorithms, as we describe next.

A. Maximum Likelihood Training

Maximum likelihood estimation (MLE) aims to find model parameters that maximize the likelihood of X . Since samples are i.i.d, the optimization criterion can be viewed as :

$$\max_{\theta \in \mathcal{F}} \mathbb{E}_{x \sim p_{real}} \log(p_\theta(x)). \quad (1)$$

It can be shown that training with the MLE criteria converges to a minimization of the KL-divergence as the sample size increases. From Eqn (1) we see that any model admitting a differentiable density $p_\theta(x)$ can be trained via backpropagation. Powerful generative models trained via MLE include Variational Autoencoders [1] and autoregressive models [19]

1) *Variational Autoencoders (VAE)*: The VAE [1] is a regularized version of the traditional autoencoder (AE). It consists of two parts : an inference network $\phi_{enc} \equiv q(z|x)$ that maps an input x to a posterior distribution of latent codes z , and a generative network $\psi_{dec} \equiv p(x|z)$ that aims to reconstruct the original input conditioned on the latent encoding. By imposing a prior distribution $p(z)$ on latent codes, this model enforces the distribution over z to be smooth and well-behaved. This property enables proper sampling from the model via ancestral sampling from latent to input space. Without it, ϕ_{enc} would encode the inputs as single points by making the variance of $q(z|x)$ arbitrarily small¹.

The full objective of the VAE is then:

$$\mathcal{L}(\theta; x) = \mathbb{E}_{q(z|x)} \log p(x|z) - KL(q(z|x)||p(z)) \leq \log p(x), \quad (2)$$

which is a valid lower bound on the true likelihood, thereby making Variational Autoencoders valid generative models. For a more in depth analysis of VAEs we refer the reader to [20].

2) *Generative Adversarial Network (GAN)*: : The GAN [2] formulates the density estimation problem as a minimax game between two opposing networks. The *generator* $G(z)$ maps noise drawn from a prior distribution p_{noise} to the input space, aiming to fool its adversary, the *discriminator* $D(x)$. The latter then tries to distinguish between real samples $x \sim p_{real}$ and fake samples $x' \sim G(z)$. In practice, both models are represented as neural networks. Formally, the objective is written as

$$\min_G \max_D \mathbb{E}_{x \sim p_{real}} \log(D(x)) + \mathbb{E}_{z \sim p_{noise}} \log(D(G(z))). \quad (3)$$

GANs have shown the ability to produce more realistic samples [21] than their MLE counterparts. However, the optimization process is notoriously difficult; stabilizing GAN training is still an open problem. In practice, GANs can also suffer from *mode collapse* [22], which happens when the generator overlooks certain modes of the target distribution.

¹In this case the model collapses to a regular autoencoder.

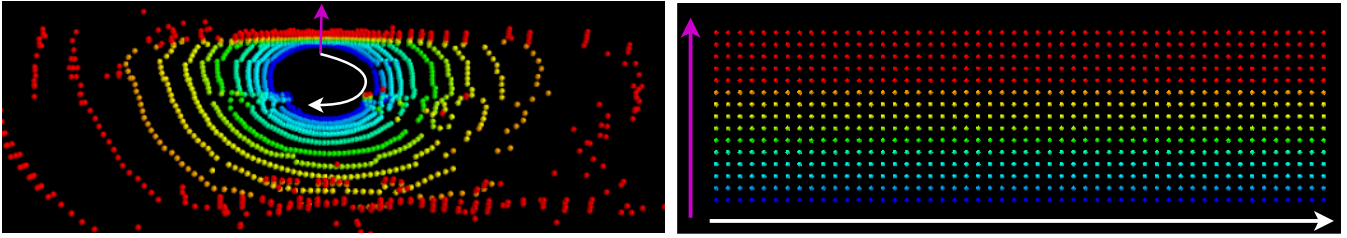


Fig. 2: Best viewed in color. Our proposed ordering of points from 3D space into a 2D grid. Points sampled from the same elevation angle share the same color. The ordering of every row is obtained by *unrolling* points in increasing azimuth angle. The showed lidar was downsampled for visual purposes.

IV. PROPOSED APPROACH FOR LIDAR GENERATION

We next describe the proposed deep learning framework used for generative modeling of lidar scans.

A. Data Representation

Our approach relies heavily on 2D convolutions, therefore we start by converting a lidar scan containing N (x, y, z) coordinates into a 2D grid. We begin by clustering together points emitted from the same elevation angle into H clusters. Second, for every cluster, we sort the points in increasing order of azimuth angle. In order to have a proper grid with a fixed amount of points per row, we divide the 360° plane into W bins. For every bin, we take the average of all its point to obtain a single representative. This yields a $H \times W \times 3$ grid, where the last axis is spatial coordinates. We note that the default ordering in most lidar scanners is the same as the one obtained after applying this preprocessing. Therefore, sorting is not required in practice, and the whole procedure can be executed in $\mathcal{O}(N)$. Figure 2 provides a visual representation of this mapping.

Since this mapping is implicitly in cylindrical coordinates (due to the ordering with respect to azimuth angle), we argue that the (x, y, z) points should also be in cylindrical form: in this representation, the convolution operator becomes fully equivariant to rotations of the (x, y) plane. Note that this is not the case when using (x, y, z) values. We later show in the experimental section that this cylindrical mapping gives better samples, while showing similar quantitative performance.

B. Training Phase

1) *VAEs*: In practice, both encoder ϕ and decoder ψ are represented as neural networks with parameters θ_{enc} and θ_{dec} respectively.

Similar to a traditional AE, the training procedure first encodes the data x into a latent representation $z = \phi(x; \theta_{enc})$. The variational aspect is introduced by interpreting z not as a vector, but as parameters of a prior distribution. In our work we choose a Gaussian $\mathcal{N}(0, 1)$ prior, and therefore z decomposes as $\mu_x, \sigma_x = \text{Chunk}(z)$.

We then sample from this distribution $\tilde{z} \sim \mathcal{N}(\mu_x, \sigma_x)$ and pass it through the decoder to obtain $\tilde{x} = \psi(\tilde{z}; \theta_{dec})$.

Using the reparametrization trick [1], the network is fully deterministic and differentiable w.r.t to its parameters θ_{enc}

and θ_{dec} , which are updated via stochastic gradient descent (SGD)

2) *GANs*: Training alternates between updates for the generator and discriminator, with parameters θ_{gen} and θ_{dis} . Similarly to the VAE, samples are obtained by ancestral sampling from the prior through the generator. In the original GAN, the discriminator’s loss is binary cross-entropy, and the generator’s is simply the opposite of its adversary. In practice, we use the Relativistic Average GAN (RaGAN) objective [23], which is easier to optimize. Further details on the importance the RaGAN loss are provided in the appendix VII-A. Again, θ_{gen} and θ_{dis} are updated using SGD.

For a complete hyperparameter list, we refer the reader to our publicly available code.²

C. Model Architecture

Deep Generative Convolutional GANs (DCGANs) [24] have shown great success in generating images. They use a symmetric architecture for the two networks: The generator consists of 5 transpose convolutions with stride two to upsample at each layer, and ReLU activations. The discriminator uses stride two convolutions to downsample the input, and Leaky ReLU activations. In both networks, Batch Normalization [25] is interleaved between convolution layers for easier optimization. We use this architecture for all our models: The VAE encoder setup is simply the first four layers of the discriminator, and the decoder’s architecture replicates the DCGAN generator.

V. EXPERIMENTS

This section provides a thorough analysis of the performance of our framework fulfilling a variety of tasks related to generative modeling. Our experiments include conditional and unconditional generation. In the first setting, the model must reconstruct a (potentially corrupted) lidar scan. In the latter setting, we are only interesting in producing realistic samples, which are not explicitly tied to a real lidar cloud.

A. Dataset

We consider the point clouds available in the KITTI dataset [26]. We use the train/validation/test set split proposed by [27], which yields 40 000, 80 and 700 samples

²https://www.github.com/pclucas14/lidar_generation

for train, validation and test sets. For training we subsample from 10z to 3hz since temporally adjacent frames are nearly identical.

B. Baseline Models

Since, to the best of our knowledge, no work has attempted generative modeling of raw lidar clouds, we compare to our method models that operate on arbitrary point clouds. We first choose AtlasNet [14], which has shown strong modeling performance on the Shapenet [28] dataset. This network first encodes point clouds using a shared *MLP* network that operates on each point *individually*. A max-pooling operation is performed on the point axis to obtain a fixed-length global representation of the point cloud. In other words, the encoder treats each point independently of other points, without assuming an ordering on the set of coordinates. This makes the feature extraction process invariant to permutations of points. The decoder is given the encoder output along with (x, y) coordinates of a 2D-grid, and attempts to *fold* this 2D-grid into a three-dimensional surface. The decoder also used a *MLP* network shared across all points.

Similar to AtlasNet, we compare our model with the one from Achlioptas et al [13]. Only its decoder differs from AtlasNet; the model does not deform a 2D grid, but rather uses fully-connected layers to convert the latent vector into a point cloud.

Both networks are trained end-to-end using the *Chamfer Loss* [16], defined as

$$d_{CH} = \sum_{x \in S_1} \min_{y \in S_2} \|x - y\|_2^2 + \sum_{y \in S_2} \min_{x \in S_1} \|x - y\|_2^2, \quad (4)$$

where S_1 and S_2 are two sets of (x, y, z) coordinates. We note again that this loss is invariant to the ordering of the output points. For both autoencoders, we regularize their latent space using a Gaussian prior to get a valid generative model.

C. Unconditional Generation

For this section, we consider the GAN model introduced in section IV-C. Our goal is to train a model that can produce realistic samples, which can be used in downstream tasks such as simulator development. In this use case, an agent operating in an environment that lacks *crispness* will likely result in poor skill transfer to real world navigation. Since the use of GANs has been shown to produce more realistic samples than MLE based models on images [29], we hope to see similar results with our model in the case of LiDAR data.

Evaluation criteria: Rigorous quantitative evaluation of samples produced by GANs and generative models is an open research question. GANs trained on images have been evaluated by the Inception Score [22] and the Frechet Inception Distance (FID) [30]. Since there exists no standardized metric for unconditional generation of lidar clouds, we rely on visual inspection of samples for quality assessment.

D. Conditional Generation

We proceed to test our approach in the conditional setting. In this setting, only the VAE model described in section IV-C is used, as vanilla GANs do not have an inference mechanism. We refer to our model as LiDAR-VAE(cyl.) and LiDAR-VAE(xyz), where the former represents its input using cylindrical coordinate, and the latter processes (x, y, z) points directly. Formally, given a lidar cloud, we evaluate a model’s ability to reconstruct it from a compressed encoding. More relevant to real world applications, we look at how robust the model’s latent representation is to input perturbation. Specifically, we look at the two following corruption mechanisms:

- **Additive Noise** : we add Gaussian noise drawn from $\mathcal{N}(0, \sigma)$ to the (x, y, z) coordinates of the lidar cloud. We experiment with varying levels of σ .
- **Data Removal** : we remove random points from the input lidar scan. Specifically, the probability of removing a point is modeled as a Bernoulli distribution parametrized by p . We experiment with different values for p .

1) *Evaluation criteria:* To measure how close the reconstructed output is to the original point cloud, we use the *Earth-Mover’s Distance* [16]. It is defined as

$$d_{EMD}(S_1, S_2) = \min_{\gamma: S_1 \rightarrow S_2} \sum_{x \in S_1} \|x - \gamma(x)\|_2 \quad (5)$$

where γ is a bijection between the two sets.

The EMD gives the solution to the solution to the optimal transportation problem, which attempts to transform one point cloud into the other. Recent work [13] has shown that this metrics correlates well with human evaluation. Moreover, this distance is sensitive to both global and local structure, and does not require points to be ordered.

E. Results

In this section, we will first discuss results for unconditional generation and subsequently evaluate results for conditional generation of lidar images.

Model	EMD
Random	7586.45
AtlasNet	5092.24
Ach. et al	2403.75
LiDAR-VAE(cyl.)	217.94
LiDAR-VAE(xyz)	208.28

TABLE I: EMD measured on test set reconstructions (lower is better)

1) *Unconditional:* From a visual inspection 6, we see that our model generates realistic samples. First, the scans have a well-defined global structure: an aerial view of the samples show points correctly align to model the structure of the road. Second, the samples share local characteristics of real data: the model correctly generates road obstacles, such as cars, or cyclists. This amounts to having locations with a dense aggregation of points, followed by a trailing area with almost

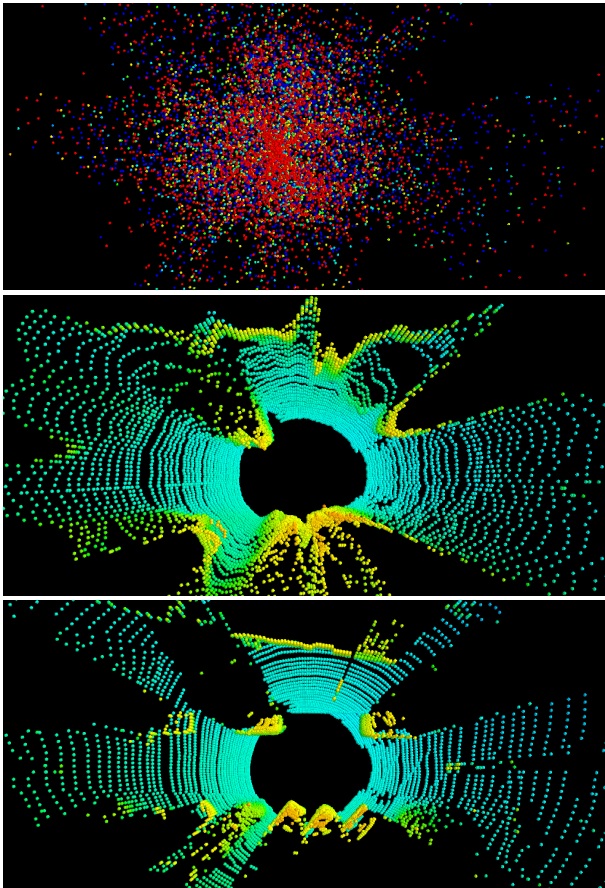


Fig. 3: Top : Corrupted lidar from the test set, where we added noise drawn from $\mathcal{N}(0, 0.1)$ on the preprocessed scan. Middle : Reconstructed point cloud given corrupted input. Bottom : original lidar scan

no points, similar to the shadow of an object. Third, model respects the point density of the data, where the density is roughly inversely proportional to the distance from the origin. Lastly, our models show good sample diversity. We refer to Figure 6 for a specific analysis of samples, and to the code repository for a wider range of samples.

2) *Conditional*: In all conditional tasks, our proposed VAE beats available baselines by a significant margin, both in terms of EMD and visual inspection. The results are described in Table 1, and in Figures 4,5. The model is able to extract a significant amount of information from noisy data. As shown in Figure 3, the VAE reconstructs correctly the defining components of the original cloud, even if the given input is seemingly uninformative. We emphasize that our model was not trained with such corrupted data, therefore these results are quite surprising.

We note that the suboptimal performance of the baselines is mainly due to two factors. First, since points are encoded independently, only information about the global structure is kept, and local fine-grained details are neglected. Second, the Chamfer Distance used for training assumes that the point cloud has a uniform density, which is not the case for lidar scans. However, we note that removing data from

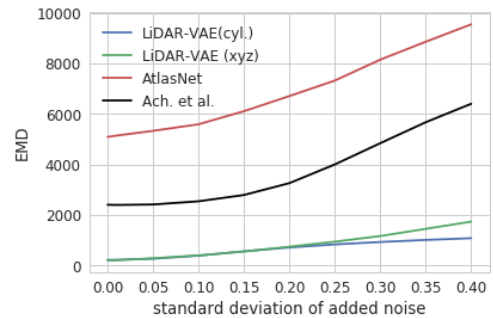


Fig. 4: EMD loss for varying levels of added noise (lower is better).

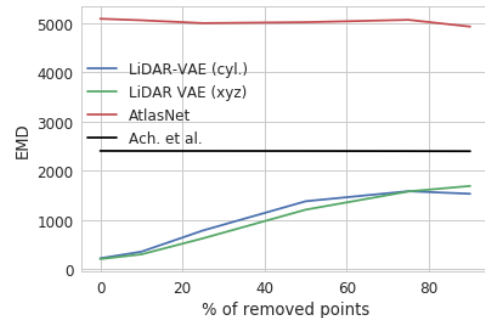


Fig. 5: EMD loss for varying levels of missing data (lower is better).

the input does not affect their reconstruction performance. By encoding points individually, their encoder can process a variable amount of points. In can therefore easily adapt to missing data. However, this characteristic is not enough to close the performance gap with our model, as shown in Figure 5.

VI. DISCUSSION AND FUTURE WORK

In this work we introduced two generative models for *raw* lidars, a GAN and a VAE. Both models use a novel lidar representation, giving rise to fully rotationally equivariant convolutions. We have shown that the proposed LiDAR-GAN can generate highly realistic data, and captures both local and global features of real lidar scans. The LiDAR-VAE successfully encodes and generates lidar samples, and is highly robust to missing or inputed data. We demonstrate that when adding enough noise to render the scan uninformative to the human eye, the proposed VAE still extracts relevant information and generates the missing data.

Moreover, we show that the LiDAR-GAN learns a meaningful latent representation. Interesting future work would be to leverage this representation for sequential data generation. In other words, one could aim to train a model such that the latent space interpolations would produce temporally adjacent frames.

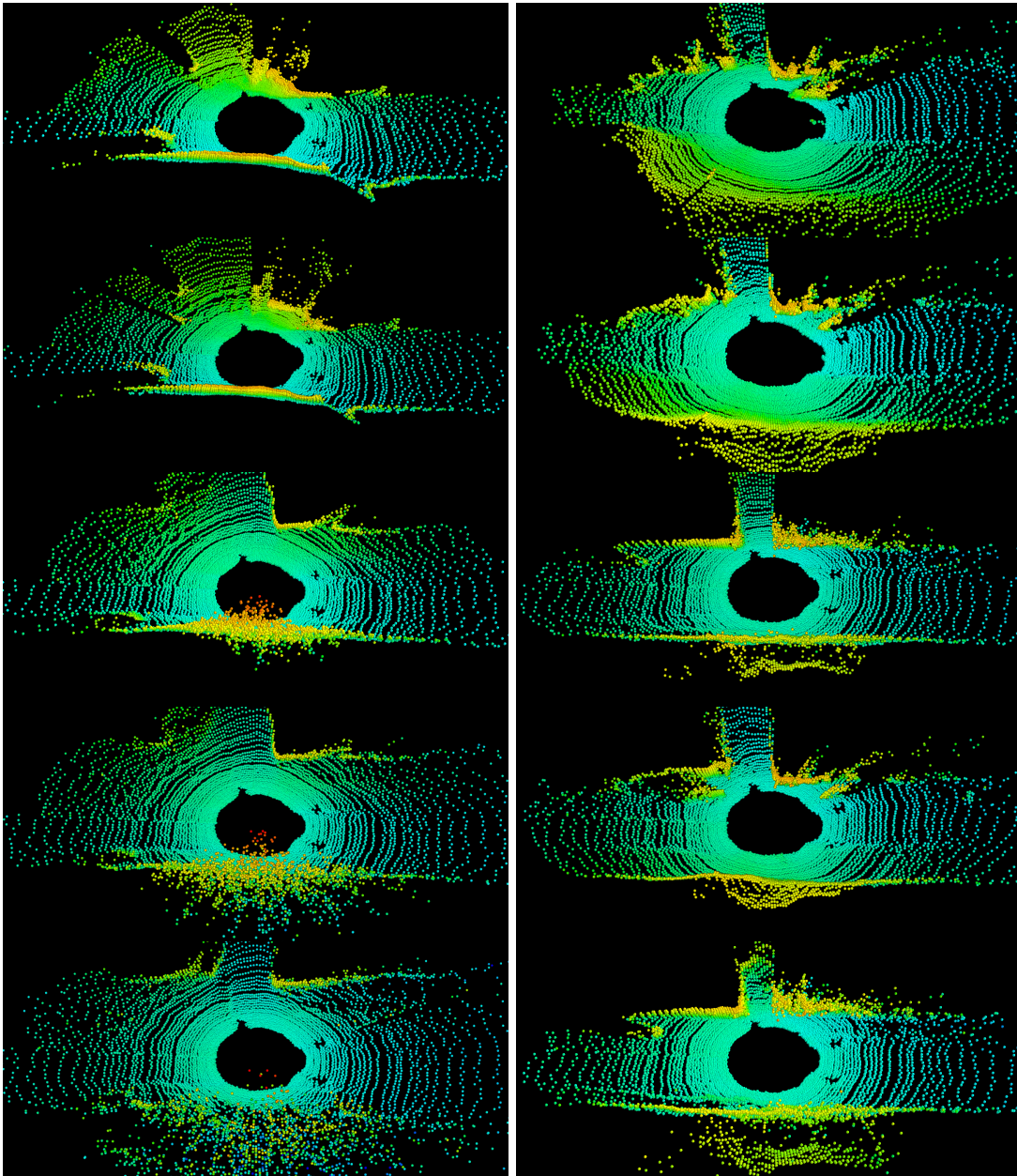


Fig. 6: Interpolations from the GAN model. For each column, we sample two noise vectors, associated to the top and bottom-most scan. We linearly interpolate between the noise vectors in latent space, giving three new noise vectors, associated with the three innermost scans. We finally push said noise through the generator to obtain the shown samples. We note that intermediate samples still look realistic.

REFERENCES

- [1] D. P. Kingma and M. Welling, "Auto-encoding variational bayes," *Proceedings of the 2nd International Conference on Learning Representations.*, 2013.
- [2] I. Goodfellow, J. Pouget-Abadie, M. Mirza, B. Xu, D. Warde-Farley, S. Ozair, A. Courville, and Y. Bengio, "Generative adversarial nets," in *Advances in neural information processing systems*, 2014, pp. 2672–2680.
- [3] A. Krizhevsky, I. Sutskever, and G. E. Hinton, "Imagenet classification with deep convolutional neural networks," in *Advances in neural information processing systems*, 2012, pp. 1097–1105.
- [4] A. Dewan, G. L. Oliveira, and W. Burgard, "Deep semantic classification for 3D lidar data," in *Intelligent Robots and Systems (IROS), 2017 IEEE/RSJ International Conference on.* IEEE, 2017, pp. 3544–3549.
- [5] Y. Zhou and O. Tuzel, "Voxelnet: End-to-end learning for point cloud based 3D object detection," *arXiv preprint arXiv:1711.06396*, 2017.
- [6] L. Caltagirone, S. Scheidegger, L. Svensson, and M. Wahde, "Fast lidar-based road detection using fully convolutional neural networks," *arXiv preprint arXiv:1703.03613*, 2017.
- [7] B. Li, "3D fully convolutional network for vehicle detection in point cloud," in *Intelligent Robots and Systems (IROS), 2017 IEEE/RSJ International Conference on.* IEEE, 2017, pp. 1513–1518.
- [8] B. Li, T. Zhang, and T. Xia, "Vehicle detection from 3D lidar using fully convolutional network," *arXiv preprint arXiv:1608.07916*, 2016.
- [9] M. Velas, M. Spanel, M. Hradis, and A. Herout, "Cnn for very fast ground segmentation in velodyne lidar data," in *Autonomous Robot Systems and Competitions (ICARSC), 2018 IEEE International Conference on.* IEEE, 2018, pp. 97–103.
- [10] V. Vaquero, I. del Pino, F. Moreno-Noguer, J. Solà, A. Sanfeliu,

- and J. Andrade-Cetto, “Deconvolutional networks for point-cloud vehicle detection and tracking in driving scenarios,” in *Mobile Robots (ECMR), 2017 European Conference on*. IEEE, 2017, pp. 1–7.
- [11] V. Vaquero, A. Sanfeliu, and F. Moreno-Noguer, “Deep lidar cnn to understand the dynamics of moving vehicles,” *arXiv preprint arXiv:1808.09526*, 2018.
- [12] P. Ondruska, J. Dequaire, D. Z. Wang, and I. Posner, “End-to-end tracking and semantic segmentation using recurrent neural networks,” *arXiv preprint arXiv:1604.05091*, 2016.
- [13] P. Achlioptas, O. Diamanti, I. Mitliagkas, and L. Guibas, “Representation learning and adversarial generation of 3D point clouds,” *arXiv preprint arXiv:1707.02392*, 2017.
- [14] T. Groueix, M. Fisher, V. G. Kim, B. C. Russell, and M. Aubry, “Atlasnet: A papier-mâché approach to learning 3D surface generation,” *arXiv preprint arXiv:1802.05384*, 2018.
- [15] Y. Yang, C. Feng, Y. Shen, and D. Tian, “Foldingnet: Point cloud auto-encoder via deep grid deformation,” in *Proc. IEEE Conf. on Computer Vision and Pattern Recognition (CVPR)*, vol. 3, 2018.
- [16] H. Fan, H. Su, and L. J. Guibas, “A point set generation network for 3D object reconstruction from a single image,” in *CVPR*, vol. 2, no. 4, 2017, p. 6.
- [17] C. R. Qi, H. Su, K. Mo, and L. J. Guibas, “Pointnet: Deep learning on point sets for 3D classification and segmentation,” *Proc. Computer Vision and Pattern Recognition (CVPR), IEEE*, vol. 1, no. 2, p. 4, 2017.
- [18] M. Arjovsky, S. Chintala, and L. Bottou, “Wasserstein gan,” *arXiv preprint arXiv:1701.07875*, 2017.
- [19] A. v. d. Oord, N. Kalchbrenner, and K. Kavukcuoglu, “Pixel recurrent neural networks,” *arXiv preprint arXiv:1601.06759*, 2016.
- [20] C. Doersch, “Tutorial on variational autoencoders,” *arXiv preprint arXiv:1606.05908*, 2016.
- [21] T. Karras, T. Aila, S. Laine, and J. Lehtinen, “Progressive growing of gans for improved quality, stability, and variation,” *arXiv preprint arXiv:1710.10196*, 2017.
- [22] T. Salimans, I. Goodfellow, W. Zaremba, V. Cheung, A. Radford, and X. Chen, “Improved techniques for training gans,” in *Advances in Neural Information Processing Systems*, 2016, pp. 2234–2242.
- [23] A. Jolicoeur-Martineau, “The relativistic discriminator: a key element missing from standard gan,” *arXiv preprint arXiv:1807.00734*, 2018.
- [24] A. Radford, L. Metz, and S. Chintala, “Unsupervised representation learning with deep convolutional generative adversarial networks,” *arXiv preprint arXiv:1511.06434*, 2015.
- [25] S. Ioffe and C. Szegedy, “Batch normalization: Accelerating deep network training by reducing internal covariate shift,” *arXiv preprint arXiv:1502.03167*, 2015.
- [26] A. Geiger, P. Lenz, C. Stiller, and R. Urtasun, “Vision meets robotics: The kitti dataset,” *The International Journal of Robotics Research*, vol. 32, no. 11, pp. 1231–1237, 2013.
- [27] W. Lotter, G. Kreiman, and D. Cox, “Deep predictive coding networks for video prediction and unsupervised learning,” *arXiv preprint arXiv:1605.08104*, 2016.
- [28] A. X. Chang, T. Funkhouser, L. Guibas, P. Hanrahan, Q. Huang, Z. Li, S. Savarese, M. Savva, S. Song, H. Su *et al.*, “Shapenet: An information-rich 3D model repository,” *arXiv preprint arXiv:1512.03012*, 2015.
- [29] A. B. L. Larsen, S. K. Sønderby, H. Larochelle, and O. Winther, “Autoencoding beyond pixels using a learned similarity metric,” *arXiv preprint arXiv:1512.09300*, 2015.
- [30] M. Heusel, H. Ramsauer, T. Unterthiner, B. Nessler, and S. Hochreiter, “Gans trained by a two time-scale update rule converge to a local nash equilibrium,” in *Advances in Neural Information Processing Systems*, 2017, pp. 6626–6637.
- [31] T. Miyato, T. Kataoka, M. Koyama, and Y. Yoshida, “Spectral normalization for generative adversarial networks,” *arXiv preprint arXiv:1802.05957*, 2018.
- [32] G. Klambauer, T. Unterthiner, A. Mayr, and S. Hochreiter, “Self-normalizing neural networks,” in *Advances in Neural Information Processing Systems*, 2017, pp. 971–980.

VII. APPENDIX

A. On the importance of Relativistic Average GAN

To stabilize GAN training, we experimented with different known tricks for image generation, namely Spectral Normalization [31], SELU activations [32] and the Relativistic Average GAN (RaGAN) loss. [23]. Of all these techniques, we found that only the RaGAN objective gave consistent improvements and stable training dynamics. RaGAN modifies equation 3 to

$$\min_G \max_{\tilde{D}} \mathbb{E}_{x \sim p_{real}} \log(\tilde{D}(x)) + \mathbb{E}_{z \sim p_{noise}} \log(\tilde{D}(G(z))).$$

where

$$\tilde{D} = \begin{cases} \text{sigmoid}(D(x) - \mathbb{E}_{x \sim p_{real}} D(x)) & \text{if disc. input is real} \\ \text{sigmoid}(D(x) - \mathbb{E}_{x \sim p_{fake}} D(x)) & \text{if disc. input is fake} \end{cases}$$

To monitor convergence, we look at the difference in discriminator output for real and fake data, shown in 7. We argue that this is a good metric for monitoring convergence, as once the discriminator correctly classifies data with 100% confidence, this metric reaches 1, and qualitative evaluation of samples suggests that they stop improving.

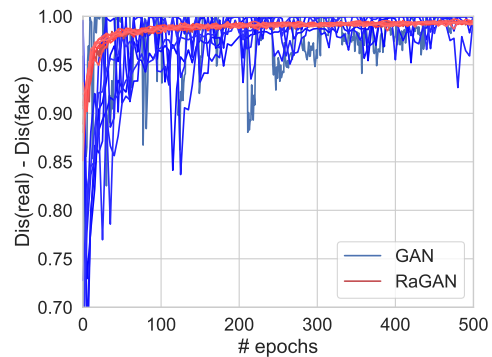


Fig. 7: Convergence analysis for 16 different runs, half of which use the RaGAN objective

In Figure 7, we plot 8 runs with the classic GAN objective, and 8 runs with the modified RaGAN objective. For each run, we sampled different hyperparameters values for the batch size, learning rates and the use of spectral normalization. These results seem to strongly suggest that the relativistic approach is much more robust to hyperparameter changes.